Comparative evaluation of photon-induced water splitting under visible light irradiation using Cd-doped TiO 2 nanoparticles and nanofibers

Nehal A. Erfan (n.erfan1@mu.edu.eg)
Minia University
Nasser A. M. Barakat
Minia University
Mohamed S. Mahmoud
Minia University

Research Article

Keywords: Cadmium, Titanium oxide, nanoparticles, nanofibers, water splitting

Posted Date: May 5th, 2022

DOI: https://doi.org/10.21203/rs.3.rs-1563496/v1

Abstract

Nanofibrous morphology and the doping technique can overcome the problem of electron/hole fast recombination and improve the activity of such important photocatalysts under visible light irradiation. In this study, nanoparticulate and nanofibrous forms of Cd-doped TiO2 were synthesized with different cadmium contents. For photocatalysts characterization, SEM, (TEM), EDX, and XRD techniques were used. The nanomorphology, cadmium content, and reaction temperature of Cd-doped TiO2 nanostructures were found to strongly affect the hydrogen production rate. Nanofibrous morphology improves the rate of hydrogen evolution by around 2,000 folds over the rate for nanoparticles, due to electron confinement in 0D nanostructures. The average rates of hydrogen production for samples of 0.5 wt% Cd are 0.7 and 16.5 ml/gcat. min for nanoparticles and nanofibers, respectively. We hypothesize that the formation of type II heterostructures between the TiO2 matrix and cadmium nanoparticles is the main reason for the observed enhancement of photocatalytic activity under visible light irradiation. Varying reaction temperature suggests that hydrogen evolution over the proposed catalyst is incompatible with the Arrhenius equation. In particular, reaction temperature was found to have a negative influence on photocatalytic activity. This work shows, for the first time, the prospects for using low-cost Cd as a co-catalyst in photon-induced water splitting and indicates a substantial enhancement in the rate of H2 production when using the Cd-doped TiO2 nanofiber photocatalyst.

1. Introduction

The depletion of fossil fuels has become a troubling fact. In addition to environmental restrictions, researchers are focusing on possible renewable energy-harvesting routes that can enable the world's energy demand to be continuously met. One such research path is to search for suitable energy carriers such as hydrogen and metals, which can be used to store renewable energy and employ it on demand. Several means of producing elemental hydrogen have been proposed, including control fermentation of waste biomasses **[1, 2]**, catalytic and thermal cracking of some hydrocarbons **[3-5]**, the use of electrical energy to extract hydrogen from water **[6],** or the use of a photocatalyst for water splitting **[7-9].**

Photocatalytic water splitting is the best strategy due to its simplicity and its favorable economic factors. In addition, if a photocatalyst that works efficiently under visible light is used, the process can be considered a renewable energy technology **[10, 11]**. Thermodynamically, in order for the redox reaction to proceed, the photcatalyst must have a conduction band with a potential level that is more negative than the redox potential of the unoccupied lowest molecular orbital of the photocatalyst-acceptor part.

To trigger the oxidation reaction, the valence band of the photocatalyst must have a potential level that is more positive than the reduction potential of the highest occupied molecular orbital in the photocatalyst-donor part. This mainly governs hydrogen and oxygen production over the surface of the photocatalyst. In other words, to start the H^+/ H_2 and O_2/ H_2O reactions, both the conduction and valence band potentials of the photocatalyst must be wider than the hydrogen and oxygen production levels (H^+/H_2 (−0.41 V vs normal hydrogen electrode (NHE) at pH 7, O_2/H_2O (+0.82 V vs NHE at pH 7)**[12]**. Among the

proposed photocatalysts for water splitting, titanium dioxide has drawn the most attention due to its low cost and high chemical stability. With its bandgap energy of 3.2 eV, TiO_2 is adequate for use under UV irradiation, however, this bandgap prevents TiO_2 activity under solar radiation because it contains only 4% UV photons **[13]**. The high photogenerated electron/hole (e/h)-pair recombination rate is another critical drawback of TiO_2, which strongly decreases its photocatalytic efficiency **[14]**. Such a fast recombination rate impedes the chemical reaction due to the short lifetime of the charge carriers (in the nanosecond range), meaning that there is not enough time for the photocatalytic reactions to take place **[15]**. Many attempts to solve these problems have been reported. The charge carriers' recombination at the grain boundaries can be strongly inhibited by controlling the internal crystalline structure to reduce the density of defects (such as TiO_2 [0 0 1] facets) **[14]**. In addition, non-metallic doping has attracted some research attention as a strategy for increasing the photo-excited electron's lifetime **[16, 17].** For enhancing TiO2 photocatalytic activity, many dopant materials such as carbonaceous materials (graphene, carbon nanotubes, fullerenes, and activated carbon) have been used **[8, 18, 19].** Furthermore, coupling with other semiconductors was proposed in order to enhance photocatalytic acivity by creating low-energy bands for the charge carriers. Typically, TiO_2 photocatalytic activity is enhanced through doping with transition metal nanoparticles. Excellent performance has been shown by such nanoparticles under UV and visible light irradiation **[20-22]**, moreover, when the nanoparticles of metal oxides are electronically doped with aliovalent dopants, oxygen vacancies, or interstitial dopants, they exhibit the same behavior as metal nanoparticles due to the substantial concentration of charge carriers over the nanoparticle surface.

Dopants in the photocatalyst act not only as recombination sites between photogenerated electrons and holes, but also as visible light absorption centers with an absorption coefficient that depends upon dopant density. Moreover, a high Schottky barrier which enhance electron capture can be obtained by doping with foreign metal nanoparticles **[23, 24]**.

Electron capture results in an enlarged separation lifetime of the e/h pair. Increasing the e/h-pair separation lifetime decimates the recombination of these pairs and therefore enhances the transfer of holes and possibly electrons to O_2 adsorbed on the TiO_2 surface. Afterwards, the excited electrons are trapped by the foreign nanoparticles and the recombination of the e/h pairs is suppressed. Moreover, some researchers have indicated that doping TiO_2 with foreign nanoparticles enhances rutile phase formation, which has a greater tendency for visible light absorption than anatase **[25, 26].** Besides the influence of the composition, the nanostructure morphology reveals a distinct effect upon the photocatalytic activity. It has been reported that the titania nanoparticles' quantum size of under 10 nm was the reason for the distinct improvement in photocatalytic activity **[27]**. The photocatalytic electronic modification and the closeness of the excited e/h pairs in nanostructures strongly contribute to the enhancement of the reaction, which consequently enhances their performances over those of larger titania powders. However, complicated and expensive processes are needed to synthesize TiO_2 quantum dots. Compared to nanoparticulate morphology, the large axial ratio of nanofibers strongly enhances the physicochemical and catalytic characteristics because of the rapid electron transfer, which markedly improves the activity of the TiO_2 photocatalyst **[25, 28]**. Among the several nanofiber synthesis

techniques, electrospinning has drawn the most attention due to its low cost, simplicity, high yield, product morphology controllability, and applicability to a wide range of materials **[28-33].** In this study, Cd-doped nanofibers were prepared by an electrospinning technique, and their photocatalytic activity for water splitting was evaluated. In addition, nanoparticulate photocatalysts with similar nanofiber compositions were prepared to study the effect of nanomorphology upon the photocatalytic activity. . Interesting results were recorded as the nanofibrous morphology strongly enhanced the photocatalytic activity. Besides the distinct enhancement in the hydrogen production rate, Cadmium doping also improved the photocatalytic splitting of water to the point that it became incompatible with the Arrhenius equation—meaning that working under low temperature is more beneficial.

2. Materials And Methods

2.1 Materials

All chemicals in this study have been used without further modification. Titanium (IV) isopropoxide and polyvinyl pyrolidone (PVP, Mw=130000) were purchased from Sigma Aldrich. Cadmium acetate di-hydrate ($Cd(CH_3CO_2)_2$ Assay 99.0%) was obtained from Showa Co. Japan. Analytical-grade ethanol was used as a solvent (Assay 99.8–100% from Alpha chemicals). Acetic acid (Assay 99–100%), sodium sulfide (Na_2SO_3, Mw=126, Assay 98%), and sodium sulfate (Na_2SO_4, Mw=78.04, Assay 55–60%) were obtained from Alpha chemicals.

2.2 Fabrication of TiO_2 and Cd-doped TiO_2 nanofibers and nanoparticles

Figure (1) represents the nanofibers and nanoparticles fabrication procedure. For comparison, pure TiO_2 nanofibers were first prepared. A mixture of 2 g anhydrous ethanol and an equal amount of glacial acetic acid was prepared. Then, 1 g of Titanium isopropoxide was added to the solvent mixture. Later on, 1 g of PVP and 6 g of ethanol mixture were added to the previous solution. The whole mixture was stirred at 300 rpm for 15 min to obtain a transparent sol–gel.

Regarding the electrospinning experiment, the unit consists of a DC power supply, a spinning syringe mounted on a flexible syringe holder, and a rotating drum target. The distance from the syringe to the rotating drum was fixed at 15 cm. To perform a uniform deposition of the nanofiber, the rotation speed of the drum target is fixed as 10 rpm. High intensity DC voltage of 20 kV is applied between the syringe tip and the rotating drum. The drum was covered by a polyethylene sheet. After electrospinning, the mat underwent a drying step under vacuum at 80 °C for 24 h, followed by a calcination process at 700 °C for a 1-h holding time. In order to prepare Cd-doped TiO_2 nanofibers, the aforementioned procedure was similarly performed after the addition of specific amounts of CdAc dissolved in 1 ml ethanol.

To prepare the final nanofibrous mats with 0.5, 1, and 2 wt% Cd, the corresponding mass of Cadmium acetate is added. Using the same prepared solutions for nanofibrous mat synthesis, nanoparticles with similar compositions were prepared by vacuously drying the solutions overnight, crushing and well

grinding before calcination process. It should be mentioned that the calcination process in the presence of CdAc should lead to thermal decomposition and production of $CdTiO_3$ over the nanofiber or nanoparticle surface **[20, 34, 35].**

The nanocomposites crystallinity is increased by increasing calcination temperature. Tryba et. al. **[36]** reported similar observations while studying the photocatalytic activity of TiO_2-WO_3 composites. Increase in crystallite size due to increase in calcination temperature is also suggested by XRD analysis performed on the nanofibers. Therefore, it can be concluded that the calcination temperature is important for the synthesis of particular morphology of TiO_2 based nanofibers.

2.3 Water photo-splitting experiment

The experiments were performed under a 1,000-W mercury lamp as a source of visible light. This lamp has been used to mimic the solar radiation in line with similar studies for the water splitting reaction **[37-39]**. It has been used to test the photocatalytic activity of the prepared nanofibers and nanoparticles in the water photo-splitting process. A solution containing 0.05 g of catalyst was added to 100 ml of 0.5 M Na_2S/Na_2SO_3 as a sacrificial agent. The general role of the scavenger agent in the water splitting process is to improve the hydrogen evolution **[20]**. The specific role of Na_2S/Na_2SO_3 sacrificing agent has been explained by **Chunxiang Li** et al **[40]**. For Na_2S/Na_2SO_3 as a sacrificial agent, they capture of holes generated from the photocatalyst which leads to promoting the oxygen evolution reaction, in turn, the hydrogen reduction reaction is enhanced as well.

The suspension was placed in a well-sealed round-bottom flask with one opening from which a rubber tube exited. This tube was immersed in a water-filled inverted graduated cylinder, by displacing the water, the evolved gases were collected. In order to maintain the reaction temperature, the round-bottom flask was jacketed by a temperature-controlled water bath, the accumulated gas from the photocatalytic water-splitting reaction consists mainly of H_2 and O_2 with a molar ratio of 2:1. The volume of accumulated hydrogen was calculated by recording the change in the volume above the water level using the following equation:

$$n = \frac{2\times273\times V}{3\times22.4\times m\times T}, \quad (1)$$

where n is the number of moles of H_2 [mmol/g], V is the volume of the gas [mL], m is the mass of the photocatalyst [g], and T is the temperature of the solution [K]. Several researchers displayed the rate of hydrogen generation in mmol/$g_{catalyst}$, µmol/h/$g_{catalyst}$, and ml/$g_{catalyst}$ **[41-43]**. According to the ideal gas law, for hydrogen gas:

0.041*V (mL)= n (mmol) (2)

Therefore, it is better to use mmol/$g_{catalyst}$ rather than ml/$g_{catalyst}$. For kinetic calculation, the rate of hydrogen evolution in mmol/min is used to calculate the quantum efficiency.

2.4 Characterization

The surface morphologies of the as-obtained nanofibers and nanoparticles was studied using the JEOL JSM-5900 scanning electron microscope (JEOL Ltd., Japan). A Rigaku X-ray diffractometer (Rigaku Co., Japan) with Cu Kα (λ=1.54056 Å) radiation over a 2θ range from 10^o to 80^o was used to characterize the phase and crystallinity of the prepared nanomaterials. A JEOL JEM-2200FS transmission electron microscope (TEM) operating at 200 kV and equipped with EDX (JEOL Ltd., Japan) was used to investigate the materials' internal structure. The absorption spectra were investigated by spectroscopic analysis using an HP 8453 UV-visible spectroscopy system, Germany. Then, the obtained figures were analyzed using the HP ChemiStation software.

3. Results And Discussion

3.1 Catalyst characterization

By choosing a suitable precursor, good nanofiber morphology can be obtained using the electrospinning technique. If an improper precursor is selected, the good morphology of the initial electrospun nanofibers can be destroyed during the calcination process. During the calcination of the electrospun nanofibers in air, the utilized polymer is fully eliminated and the metallic precursor decomposes into its most stable form. The main aspect of a proper precursor is polycondensation during sol–gel preparation. The high polycondensation tendency and hydrolysis reactions for alkoxides explain their distinct performance in forming an integrated network **[44-46].**

The organometallic family comprises compounds having one or more metal atoms in the molecule, and metal alkoxides are members of that family. Metal alkoxides (R-O-M) were obtained by replacing the hydrogen atom in the hydroxyl group of alcohols (R-OH) with a metal atom M, which are the class of chemical precursors most widely used in sol–gel formation because of their condensation behavior and tendency to combine together to form a gel network. The gel network can be formed using metal salts such as chlorides, nitrates, and acetates besides alkoxides. The acetates showed the most convenient polycondensation behavior for gel network formation. The excellent morphology and bead-free nanofibers shown in Fig. 1A indicate that the electrospinning working parameters and the composition of the utilized sol–gel were properly selected. As a result of the polycondensation behaviors of all utilized precursors, the calcination process had no effect upon the nanomaterials' morphology.

It is notable that the addition of cadmium acetate did not affect the general morphology of the obtained nanofibers, however, the addition of cadmium distinctly affected the obtained nanofibers' morphology. The nanofiber sample chosen for SEM imaging is that having a composition of 0.5 wt% Cd-doped TiO_2 nanofibers, presenting the best photocatalytic performance under visible light irradiation. As observed in Figs. 2B and C, cadmium incorporation results in the breaking of nanofibers. The produced nanofibers

length decrease by increasing the cadmium content in the initial electrospinning solution and acetate ions decomposition. Typically results in evolving CO_2 and methane gases leaving behind holes on the surface, potentially explaining the nanofiber breakdown. Comparing Fig. 2B to 2A, the addition of cadmium can be seen to result in the creation of rough surface nanofibers. By contrast, the cadmium-free nanofibers have a smooth surface. A high surface area is a preferable characteristic for a photocatalyst, as it leads to enhanced photon absorption and consequently increases the catalytic activity.

Figure 2D shows the TEM image of the Cd-doped TiO_2 nanofiber, the appearance of transparent CdTiO3 bubble-like nanoparticles attached to the surface of the TiO_2 nanofiber is notable. As CdTiO3 nanoparticles exhibit several catalytic, optical, and electrical properties, their presence over the surface of the nanofiber can enhance the TiO_2 nanofiber's photocatalytic performance by functioning as electron trapping sites for the hydrogen evolution reaction, as will be discussed below.

Figure 3 displays the TEM and the EDX results for the Cd-doped TiO_2 nanoparticles. The $CdTiO_3$ phase clearly appears in the TiO_2 matrix. As shown in the Figure, $CdTiO_3$ has a different structure than that of TiO_2 (Fig. 3B), which confirms the formation a Cd-doped TiO_2 nanostructure. The EDX result (Fig. 3C) confirms the presence of Cd in the TiO_2 matrix.

X-ray diffraction analysis is a typical technique for determining the compositions of crystalline materials. Basically, brookite, anatase, and rutile are common TiO_2 phases from a crystal structure point of view, the latter two are abundantly found. Figure 4 represents the impact of cadmium doping on the crystal structure of the produced nanofibers. Cd-free electrospun nanofibers consist entirely of the anatase phase, the diffraction peaks appear at 2θ values of 25.09°, 37.65°, 38.44°, 47.89°,53.89°, 55.07°, 62.40°, 68.70°, 70.04°, and 75.00° and correspond to the (101), (004), (112), (200), (105), (211), (204), (220), (220), and (215) crystal planes, respectively. This suggests the formation of pure anatase TiO_2 according to the XRD database (JCPDS card no 21-1272). One peak refers to the rutile phase at a 2θ value of 27.4 detected in the 0% Cd nanofiber sample. It is well-known that metal oxides can form chemical compound alloys. As can be seen in Fig. 4, CdAc addition enhanced the rutile phase formation, which compared to anatase, has a greater tendency for visible light absorption **[25, 26]**. The tetragonal rutile phase (JCPDS 21-1276) at 2θ values of 27.4°, 36.1°, 39.2°, 41.2°, 44.1°, 54.3°, 56.6°, 62.7°, 64°, 69°, and 69.8° corresponds to the (110), (101), (200), (111), (210), (211), (220), (002), (310), (301), and (112) crystal planes, respectively. These results indicate that the amount of rutile phase increases with increasing cadmium content in the produced nanofibers. The rutile phase peak intensity decreases by increasing Cd content. The reason for this may be that the addition of foreign dopant atoms into the lattice weakens its structure, thereby decreasing crystallinity **[46].** The rutile (110) peaks shift towards lower angle for the samples with the addition of Cadmium in addition to Cadmium smaller radii compared to radius of Ti^{+4} indicating the incorporation of Cadmium metal ions in the TiO_2 matrix.

As observed in Fig. 4, Cd was dissolved in TiO_2 to form cadmium titanate ($CdTiO_3$). Diffraction peaks indicating $CdTiO_3$ formation were observed at 31.1°, 34.2°, 46.9°, and 59.3°, corresponding to the (101),

(104), (110), (024), and (214) crystal planes, respectively (JCPDS card no. 29-0277). Those peaks appeared at high concentrations of Cd-doped nanofibers (1 and 2%), while the $CdTiO_3$ phase cannot be observed in 0.5 wt% Cd nanofiber. This may be due to polymer encapsulation at low Cd content. The XRD result for Cd-doped TiO_2 nanoparticles shows a similar pattern to the nanofibers, as the XRD result does not depend upon the nanostructure's morphology (Fig. 3B).

3.2 Photocatalytic activity investigation

Figure 5 represents the effect of cadmium content upon the amount of hydrogen evolved under visible light irradiation using the prepared Cd-doped nanoparticles and nanofibers. The hydrogen production rates for the 2 wt% Cd samples were 27 and 250 ml $H_2/g_{cat.}$ for nanoparticles and nanofibers, respectively. The nanofibrous morphology distinctly enhanced its photocatalytic activity. As observed in the Figure, the rate of hydrogen production was increased greatly using nanofibers compared to nanoparticles at the same composition. The structure that provides one dimension for electron motion may be the reason for the considerable enhancement in the nanofibers' photocatalytic activity, however, in the nanoparticles with 0D structure, full electron confinement takes place, which favors the e/h recombination reaction **[47]**. Moreover, the results show the effect of cadmium doping upon the photocatalytic activity. As shown in Fig. 5, a remarkable enhancement in the photocatalytic activity of TiO_2 was detected after the addition of small amounts of cadmium. In fact, cadmium particles act not only as visible light absorption centers with an absorption coefficient dependent on Cd density, but also as recombination sites between photogenerated electrons and holes. Moreover, doping by Cadmium nanoparticles yields a higher Schottky barrier that increases electron capture **[24]**. This electron capture results in an increased e/h—pair separation lifetime, which consequently suppresses the recombination of e/h pairs. Decimating e/h-pair recombination enhances the hole transfer and perhaps O_2 adsorption on the TiO_2 surface. The observed decrease in the photocatalytic activity of the nanofibers for Cd concentrations above 0.5 wt% is related to the decrease in rutile phase intensity, as confirmed by XRD results (Fig. 4).

Basically, the photocatalytic activity is intensely related to the optical properties of the light source used in the experiments, like the light intensity and irradiation area. Hence, the catalyst activities cannot be compared with each other if the reaction conditions are different from each other. Therefore, determination of an apparent quantum yield (AQY), which rules the effect of light source out, is essential. Accordingly, It is necessary to determine the efficiency (AQY) of the present system and compare with other published works. To judge the feasibility of a proposed photocatalyst, the quantum efficiency of H_2 evolution is calculated as follows:

$$\eta = \frac{N_e}{N_v}, \qquad (2)$$

where η is the energy conversion efficiency, N_e is the number of electrons involved in the hydrogen evolution reaction, and N_v is the number of incident photons in the reaction area. N_e can be calculated from the rate of hydrogen evolution (from Fig. 5, production rate= 0.63 mmol H_2 $g^{-1}_{catalyst}min^{-1}$ for Cd-doped TiO_2 nanoparticles).

Through those rates, the actual number of electrons disappearing due to the hydrogen evolution reaction can be obtained, meanwhile, the number of incident photons (N_v) is calculated as

$$N_v = \frac{I}{E_v} \quad (3)$$

where I is the solar intensity in the El Minia Governorate, Egypt (Latitude: 31° 25`, I= 258–266.7 Wm^{-2} **[48]**) and E_v is the photon energy (3.97×10^{-19}, J $photon^{-1}$). Accordingly, the photon flux intensity is 6.51×10^{20} photons/s m^2 solar. This calculation indicates that the prepared catalyst has achieved a 20 % conversion of photons to electrons, showing that the Cd-doped TiO_2 nanostructure photocatalyst is capable of increasing the absorbance of photons and prolonging the lifetime for e/h pairs.

Instead, researchers used another practical standard to calculate the efficiency of the photocatalystic water splitting, namely solar-to-hydrogen (STH) efficiency. It can be calculated using the following formula:

$$STH = \frac{Energy\ released\ from\ H_2\ gas}{Incident\ solar\ energy} = \frac{r_{H_2}\Delta G}{I_S A_r} \quad (4)$$

where r_{H_2} is the hydrogen production rate in mol/s, ΔG is the Gibbs free energy associated with hydrogen gas in J/mol, I_s is the solar energy flux in (W/cm^2), and A_r is the surface area of the photocatalytic reactor. Using the STH formula, the STH efficiency of the prepared Cd-doped TiO_2 nanoparticles is calculated to be 0.64% and 9% for Cd-doped TiO_2 nanoparticle and Cd-doped TiO_2 nanofiber, respectively. Table 1 shows the rate of hydrogen evolution of this study compared with other works. It is important to note that comparison of the rate of hydrogen evolution should be done for experiments that are conducted using same light source and same sacrificing agent. However, it is hard to fulfill that condition to compare our results with other works. For nanostructures containing TiO_2, it is apparent that the moles of hydrogen produced by the Cd–TiO_2 nanofibers prepared in this study is relatively higher than that obtained previously by other scholars (Table 1), the exception is Mohamed et al. **[20],** who indicated that a Cd-doped TiO_2 nanotube can achieve 24 mmol $H_2/g_{cat.}$ min using methanol as a scavenger agent. This reveals that the Cd-doped TiO_2 nanofiber may act as an effective photocatalyst candidate for the photon-induced water-splitting reaction. However, the stability and recyclability of this substance must be considered in greater detail before nominating it as a viable photocatalyst.

Table 1: A comparison of the hydrogen evolution rate for different nanocatalysts

No	Photocatalyst	Light source	Scavenger agent	Hydrogen production rate mmol $H_2/g_{cat.}$ min	Ref./year
1	Pt/ TiO_2 nanosheet	Xenon Arc lamb 350 W	Ethanol	0.0056	**[49]**/2010
2	Graphene modified TiO_2 nanoparticles	Xenon Arc lamb 350 W	Methanol	0.0123	**[50]**/2011
3	TiO_2 nanoparticles	Xenon lamb 150 W	Methanol	0.1	**[51]**/2014
4	(Pt/HS-TiO_2)	Mercury lamb 400 W	Methanol	0.017	**[52]**/2016
5	Pt-doped TiO_2–ZnO	Mercury lamb 400 W	Methanol	0.0034	**[53]**/2017
6	Pt-TiO_2 particles	Mercury lamb 450 W	Methanol	0.444	**[54]/2005**
6	Cd-doped TiO_2 nanotube	Mercury lamb 1000 W	Methanol	24	**[20]**/2018
7	CdS/TiO_2 mesoporous core-shell	Sunlight	Na_2S/Na_2SO_3	1.13	**[21]**/2018
8	Ni/TiO_2 nanotube	Solar simulator Xenon lamb	-	0.433	**[22]**/2019
9	Ni/GO-TiO_2 nanoparticles	Sunlight	Methanol	3	**[55]**/2019
10	Ag-TiO2 NF	Mercury lamb 1000 W	Na_2S/Na_2SO_3	2	**[56]**/2020
11	$NiCo_2S_4$/CdO@CC	Sunlight	-	0.00125	**[57]**/2020
12	Cd-doped TiO_2 nanoparticles Cd-doped TiO_2 nanofibers	Mercury lamb 1000 W	Na_2S/Na_2SO_3	0.7 16.5	This study

3.3 Influence of reaction temperature

The kinetic energy can be measured by the temperature of the system, so higher temperature leads to a higher average molecular kinetic energy and more collisions per unit time. Therefore, in most chemical

reactions, the temperature has a positive effect upon the reaction rates, however, nanostructures frequently show unexpected behaviors.

Figure 6 shows water photo splitting at temperatures of 298, 308, and 318 K. The results indicate that the hydrogen production rate decreases with increasing reaction temperature using Cd-doped TiO_2 nanofibers (0.5 wt% sample) as a photocatalyst. This behavior may be because of the negative impact of the temperature upon the metal's electrical conductivity as increasing temperature increases the electrons' kinetic energy and disordering. This kinetic energy can move the reactant molecules away from the active zones. In addition, other researchers have noted that a surface plasmon is remarkably observed at low temperatures **[58].** Moreover, increasing the temperature can increase the possibility of recombination between the charge holders, which consequently decreases the semiconductor's photoactivity.

Therefore, we theoretically project that increasing the temperature is not preferred in the water-splitting reaction. This hypothesis has been verified experimentally (Fig. 6). Numerically, the hydrogen production rates are 350, 300, and 100 ml/ g_{cat} at reaction temperatures of 298, 308, and 318 K, respectively. This finding confirms that the water-splitting reaction over the proposed catalyst surface does not follow the Arrhenius equation. Obtaining a high yield at low temperatures is an economically preferred characteristic in industrial settings.

4. Conclusions

This study presented the preparation, characterization, and examination of Cd-doped TiO_2 nanoparticles and nanofibers as stable and nonprecious catalysts for water-splitting reactions. The structure of the photocatalysts was verified by SEM, TEM, EDS, and XRD. The UV-visible spectrum indicated that Cd-doping for TiO_2 nanofibers does not affect the optical properties of TiO_2, the bandgap remained nearly constant at 2.93 eV, and application of the catalyst showed enhanced production of hydrogen in the case of 2 wt.% Cd-doped TiO_2 nanoparticles and 0.5 wt% Cd-doped TiO_2 nanofibers. Although doping by Cd does not have a considerable impact upon the bandgap, it shows a good influence on increasing the electron/hole lifetime. Accordingly, it presented good photocatalytic activity for water splitting, as concluded by the distinct increase in the hydrogen evolution rate compared to that of undoped titanium oxide nanoparticles and nanofibers.

Declarations

-Authors contributions

Nehal A. Erfan: Wrote the manuscript, helped in the experimental work, did the analysis process, explained the results and manipulated the data results.

N. A. M. Barakat: planned the experimental work, helped in explaining the results and data analysis.

Mohamed S. Mahmoud: helped in writing the manuscript and did the review process for the manuscript.

-Ethics approval and consent to participate

Not applicable

-Consent for publication

Not applicable

-Competing interests

I declare that the authors have no competing interests as defined by Springer, or other interests that might be perceived to influence the results and/or discussion reported in this paper.

-Availability of data and materials

The results/data/figures in this manuscript have not been published elsewhere, nor are they under consideration (from you or one of your Contributing Authors) by another publisher.

All of the material is owned by the authors and/or no permissions are required.

-Funding

Not applicable

References

1. S.-K. Han, H.-S.J.I.j.o.h.e. Shin, Biohydrogen production by anaerobic fermentation of food waste, 29 (2004) 569-577.
2. D.B. Levin, L. Pitt, M.J.I.j.o.h.e. Love, Biohydrogen production: prospects and limitations to practical application, 29 (2004) 173-185.
3. W. Grochala, P.P.J.C.r. Edwards, Thermal decomposition of the non-interstitial hydrides for the storage and production of hydrogen, 104 (2004) 1283-1316.
4. T. Zhang, M.D.J.A.C.A.G. Amiridis, Hydrogen production via the direct cracking of methane over silica-supported nickel catalysts, 167 (1998) 161-172.
5. A.M. Amin, E. Croiset, W.J.I.J.o.H.E. Epling, Review of methane catalytic cracking for hydrogen production, 36 (2011) 2904-2935.
6. K. Zeng, D.J.P.i.e. Zhang, c. science, Recent progress in alkaline water electrolysis for hydrogen production and applications, 36 (2010) 307-326.
7. M. Ni, M.K. Leung, D.Y. Leung, K.J.R. Sumathy, S.E. Reviews, A review and recent developments in photocatalytic water-splitting using TiO2 for hydrogen production, 11 (2007) 401-425.

8. N.A. Barakat, E. Ahmed, M.T. Amen, M.A. Abdelkareem, A.J.M.L. Farghali, N-doped Ni/C/TiO2 nanocomposite as effective photocatalyst for water splitting, 210 (2018) 317-320.
9. M.S. Mahmoud, E. Ahmed, A. Farghali, A. Zaki, N.A.J.M.C. Barakat, Physics, Synthesis of Fe/Co-doped titanate nanotube as redox catalyst for photon-induced water splitting, 217 (2018) 125-132.
10. S.M. Kotay, D.J.I.J.o.H.E. Das, Biohydrogen as a renewable energy resource—prospects and potentials, 33 (2008) 258-263.
11. C. Perkins, A.W. Weimer, Solar-thermal production of renewable hydrogen, 55 (2009) 286-293.
12. B.-J. Ng, L.K. Putri, X.Y. Kong, Y.W. Teh, P. Pasbakhsh, S.-P. Chai, Z-Scheme Photocatalytic Systems for Solar Water Splitting, Advanced Science, 7 (2020) 1903171.
13. A. Bumajdad, M.J.P.C.C.P. Madkour, Understanding the superior photocatalytic activity of noble metals modified titania under UV and visible light irradiation, 16 (2014) 7146-7158.
14. W.-J. Ong, L.-L. Tan, S.-P. Chai, S.-T. Yong, A.R.J.N. Mohamed, Highly reactive {001} facets of TiO 2-based composites: synthesis, formation mechanism and characterization, 6 (2014) 1946-2008.
15. M.N. Chong, B. Jin, C.W. Chow, C.J.W.r. Saint, Recent developments in photocatalytic water treatment technology: a review, 44 (2010) 2997-3027.
16. X. Pan, M.-Q. Yang, X. Fu, N. Zhang, Y.-J.J.N. Xu, Defective TiO 2 with oxygen vacancies: synthesis, properties and photocatalytic applications, 5 (2013) 3601-3614.
17. D.-H. Wang, L. Jia, X.-L. Wu, L.-Q. Lu, A.-W.J.N. Xu, One-step hydrothermal synthesis of N-doped TiO 2/C nanocomposites with high visible light photocatalytic activity, 4 (2012) 576-584.
18. Y. Zhang, Z.-R. Tang, X. Fu, Y.-J.J.A.n. Xu, Engineering the unique 2D mat of graphene to achieve graphene-TiO2 nanocomposite for photocatalytic selective transformation: what advantage does graphene have over its forebear carbon nanotube?, 5 (2011) 7426-7435.
19. R. Leary, A.J.C. Westwood, Carbonaceous nanomaterials for the enhancement of TiO2 photocatalysis, 49 (2011) 741-772.
20. M.S. Mahmoud, E. Ahmed, A.A. Farghali, A.H. Zaki, E.A.M. Abdelghani, N.A.M. Barakat, Influence of Mn, Cu, and Cd–doping for titanium oxide nanotubes on the photocatalytic activity toward water splitting under visible light irradiation, Colloids and Surfaces A: Physicochemical and Engineering Aspects, 554 (2018) 100-109.
21. H.H. El-Maghrabi, A. Barhoum, A.A. Nada, Y.M. Moustafa, S.M. Seliman, A.M. Youssef, M. Bechelany, Synthesis of mesoporous core-shell CdS@TiO2 (0D and 1D) photocatalysts for solar-driven hydrogen fuel production, Journal of Photochemistry and Photobiology A: Chemistry, 351 (2018) 261-270.
22. Z. Dong, D. Ding, T. Li, C. Ning, Facile preparation of Ti3+/Ni co-doped TiO2 nanotubes photoanode for efficient photoelectrochemical water splitting, Applied Surface Science, 480 (2019) 219-228.
23. A. Agrawal, R.W. Johns, D.J. Milliron, Control of Localized Surface Plasmon Resonances in Metal Oxide Nanocrystals, Annual Review of Materials Research, 47 (2017) 1-31.

24. A. Vorontsov, I. Stoyanova, D. Kozlov, V. Simagina, E.J.J.o.c. Savinov, Kinetics of the photocatalytic oxidation of gaseous acetone over platinized titanium dioxide, 189 (2000) 360-369.
25. N.A. Barakat, M.A. Kanjwal, I.S. Chronakis, H.Y.J.J.o.M.C.A.C. Kim, Influence of temperature on the photodegradation process using Ag-doped TiO2 nanostructures: negative impact with the nanofibers, 366 (2013) 333-340.
26. M.S. Hassan, T. Amna, D.R. Pandeya, A.M. Hamza, Y.Y. Bing, H.-C. Kim, M.-S. Khil, Controlled synthesis of Mn□O□ nanowires by hydrothermal method and their bactericidal and cytotoxic impact: a promising future material, Appl Microbiol Biotechnol, 95 (2012) 213-222.
27. M. Anpo, T. Shima, Y.J.C.L. Kubokawa, ESR and photoluminescence evidence for the photocatalytic formation of hydroxyl radicals on small TiO2 particles, 14 (1985) 1799-1802.
28. N.A. Barakat, M.A. Abdelkareem, M. El-Newehy, H.Y.J.N.r.l. Kim, Influence of the nanofibrous morphology on the catalytic activity of NiO nanostructures: an effective impact toward methanol electrooxidation, 8 (2013) 1-6.
29. N. Barakat, M. Nassar, T. Farrag, M.J.E.S. Mahmoud, P. Research, Effective photodegradation of methomyl pesticide in concentrated solutions by novel enhancement of the photocatalytic activity of TiO 2 using CdSO 4 nanoparticles, 21 (2014) 1425-1435.
30. N.A.J.M.L. Barakat, Effective Co–Mn–O nanofibers for ammonia borane hydrolysis, 106 (2013) 229-232.
31. N.A.M. Barakat, Catalytic and photo hydrolysis of ammonia borane complex using Pd-doped Co nanofibers, Applied Catalysis A: General, 451 (2013) 21-27.
32. N.A. Barakat, M. Abadir, F.A. Sheikh, M.A. Kanjwal, S.J. Park, H.Y.J.C.e.j. Kim, Polymeric nanofibers containing solid nanoparticles prepared by electrospinning and their applications, 156 (2010) 487-495.
33. N.A.M. Barakat, M.A. Abdelkareem, H.Y. Kim, Ethanol electro-oxidation using cadmium-doped cobalt/carbon nanoparticles as novel non precious electrocatalyst, Applied Catalysis A: General, 455 (2013) 193-198.
34. R.M. Mahfouz, G.A.W. Ahmed, T. Al-Rashidi, Effect of surfactant-free addition and γ-irradiation on the synthesis of CdO quantum dots by thermal decomposition of γ-irradiated anhydrous cadmium acetate, Cogent Chemistry, 2 (2016) 1215233.
35. A. Tadjarodi, M. Imani, H. Kerdari, Application of a facile solid-state process to synthesize the CdO spherical nanoparticles, International Nano Letters, 3 (2013) 43.
36. B. Tryba, M. Piszcz, A.W. Morawski, Photocatalytic activity of TiO2-WO3 composites, Int. J. Photoenergy (2009), https://doi.org/10.1155/2009/297319.
37. Fujihara, K., Ohno, T., Matsumura, M. Splitting of water by electrochemical combination of two photocatalytic reactions on TiO2 particles. *J. Chem. Soci. Faraday Trans.* 1998, *94*, 3705–3709.
38. Sayama, K., Arakawa, H., Domen, K. Photocatalytic water splitting on nickel intercalated A(4)Ta(*x*)Nb(6−*x*)O(17) (A = K, Rb). *Cataly. Today* 1996, *28*, 175–182.

39. Kudo, A., Kato, H., Nakagawa, S. Water Splitting into H2 and O2 on New Sr2M2O7 (M = Nb andTa) Photocatalysts with Layered Perovskite Structures: Factors Affecting the Photocatalytic Activity*. J. Phys. Chem. B* 1999, *104*, 571–575.
40. Li, C., Hu, P., Meng, H. *et al.* Role of Sulfites in the Water Splitting Reaction. *J Solution Chem* 45, 67–80 (2016). https://doi.org/10.1007/s10953-015-0422-1
41. Sayama, K., Arakawa, H. Effect of carbonate salt addition on the photocatalytic decomposition of liquid water over Pt-TiO2 catalyst*. J. Chem. Soc.-Faraday Trans.* 1997, *93*, 1647–1654.
42. H. Dang, X. Dong, Y. Dong, Y. Zhang, S. Hampshire, Int. J. Hydrogen Energy 38(2013) 2126–2135.
43. J. Liu, G. Liu, M. Li, W. Shen, Z. Liu, J. Wang, J. Zhao, L. Jiang and Y. Song, *Energ. Environ. Sci.*, 2010, 3, 1503-0506.
44. N.A. Barakat, A. Taha, M. Motlak, M.M. Nassar, M. Mahmoud, S.S. Al-Deyab, M. El-Newehy, H.Y.J.A.C.A.G. Kim, ZnO&Fe2O3-incoportaed TiO2 nanofibers as super effective photocatalyst for water splitting under visible light radiation, 481 (2014) 19-26.
45. A.V. Rupa, D. Divakar, T.J.C.I. Sivakumar, Titania and noble metals deposited titania catalysts in the photodegradation of tartazine, 132 (2009) 259-267.
46. S. Chuangchote, J. Jitputti, T. Sagawa, S.J.A.a.m. Yoshikawa, interfaces, Photocatalytic activity for hydrogen evolution of electrospun TiO2 nanofibers, 1 (2009) 1140-1143.
47. J. Yu, Q. Xiang, M.J.A.C.B.E. Zhou, Preparation, characterization and visible-light-driven photocatalytic activity of Fe-doped titania nanorods and first-principles study for electronic structures, 90 (2009) 595-602.
48. D.L. Schodek, P. Ferreira, M.F. Ashby, Nanomaterials, nanotechnologies and design: an introduction for engineers and architects, Butterworth-Heinemann, 2009.
49. M. Bady, Towards Sustainable Power Generation Using Solar Chimney %J Open Access Library Journal, Vol.02No.04 (2015) 9.
50. J. Yu, L. Qi, M. Jaroniec, Hydrogen Production by Photocatalytic Water Splitting over Pt/TiO2 Nanosheets with Exposed (001) Facets, The Journal of Physical Chemistry C, 114 (2010) 13118-13125.
51. Q. Xiang, J. Yu, M.J.N. Jaroniec, Enhanced photocatalytic H 2-production activity of graphene-modified titania nanosheets, 3 (2011) 3670-3678.
52. Y. Zhang, Structural evolution from TiO nanoparticles to nanosheets and their photocatalytic performance in hydrogen generation and environmental pollution removal, RSC advances, v. 4 (2014) pp. 16146-16152-12014 v.16144 no.16131.
53. Z. Zhu, C.-T. Kao, B.-H. Tang, W.-C. Chang, R.-J. Wu, Efficient hydrogen production by photocatalytic water-splitting using Pt-doped TiO2 hollow spheres under visible light, Ceramics International, 42 (2016) 6749-6754.
54. M.-Y. Xie, K.-Y. Su, X.-Y. Peng, R.-J. Wu, M. Chavali, W.-C. Chang, Hydrogen production by photocatalytic water-splitting on Pt-doped TiO2–ZnO under visible light, Journal of the Taiwan

Institute of Chemical Engineers, 70 (2017) 161-167.
55. Anna Galińska and Jerzy Walendziewski, Photocatalytic Water Splitting over Pt–TiO2 in the Presence of Sacrificial Reagents, Energy Fuels 2005, 19, 3, 1143–1147
56. M.S. Atrees, E.E. Ebraheim, M.E.M. Ali, Y.M. Khawassek, M.S. Mahmoud, M.M. Almutairi, Synergetic effect of metal-doped GO and TiO2 on enhancing visible-light-driven photocatalytic hydrogen production from water splitting, Energy Sources, Part A: Recovery, Utilization, and Environmental Effects, (2019) 1-11.
57. N.A.M. Barakat, N.A. Erfan, A.A. Mohammed, S.E.I. Mohamed, Ag-decorated TiO2 nanofibers as Arrhenius equation-incompatible and effective photocatalyst for water splitting under visible light irradiation, Colloids and Surfaces A: Physicochemical and Engineering Aspects, (2020) 125307.
58. H. Anwer, H. Lee, H.-R. Kim, H.-K. Kim, J.-W. Park, Selective transport and separation of charge–carriers by an electron transport layer in NiCo2S4/CdO@CC for excellent water splitting, Applied Catalysis B: Environmental, 265 (2020) 118564.
59. Y. Xia, D.J.J.J.o.c.e. Campbell, Plasmons: why should we care?, 84 (2007) 91.
60. T. Luttrell, S. Halpegamage, J. Tao, A. Kramer, E. Sutter, M.J.S.r. Batzill, Why is anatase a better photocatalyst than rutile?-Model studies on epitaxial TiO 2 films, 4 (2014) 1-8.
61. D. Reyes-Coronado, G. Rodríguez-Gattorno, M. Espinosa-Pesqueira, C. Cab, R.d. de Coss, G.J.N. Oskam, Phase-pure TiO2 nanoparticles: anatase, brookite and rutile, 19 (2008) 145605.
62. L. Liu, H. Zhao, J.M. Andino, Y.J.A.C. Li, Photocatalytic CO2 reduction with H2O on TiO2 nanocrystals: Comparison of anatase, rutile, and brookite polymorphs and exploration of surface chemistry, 2 (2012) 1817-1828.
63. D.O. Scanlon, C.W. Dunnill, J. Buckeridge, S.A. Shevlin, A.J. Logsdail, S.M. Woodley, C.R.A. Catlow, M.J. Powell, R.G. Palgrave, I.P.J.N.m. Parkin, Band alignment of rutile and anatase TiO 2, 12 (2013) 798-801.
64. T. Umebayashi, T. Yamaki, S. Yamamoto, A. Miyashita, S. Tanaka, T. Sumita, K. Asai, Sulfur-doping of rutile-titanium dioxide by ion implantation: Photocurrent spectroscopy and first-principles band calculation studies, Journal of Applied Physics, 93 (2003) 5156-5160.
65. N.A.M. Barakat, M.S. Khil, F.A. Sheikh, H.Y. Kim, Synthesis and Optical Properties of Two Cobalt Oxides (CoO and Co3O4) Nanofibers Produced by Electrospinning Process, The Journal of Physical Chemistry C, 112 (2008) 12225-12233.
66. N.A.M. Barakat, K.-D. Woo, S.G. Ansari, J.-A. Ko, M.A. Kanjwal, H.Y. Kim, Preparation of nanofibers consisting of MnO/Mn3O4 by using the electrospinning technique: the nanofibers have two band-gap energies, Applied Physics A, 95 (2009) 769-776.
67. S. Zhu, S. Liang, Q. Gu, L. Xie, J. Wang, Z. Ding, P. Liu, Effect of Au supported TiO2 with dominant exposed {001} facets on the visible-light photocatalytic activity, Applied Catalysis B: Environmental, 119-120 (2012) 146-155.
68. J. Low, J. Yu, M. Jaroniec, S. Wageh, A.A. Al-Ghamdi, Heterojunction Photocatalysts, Advanced Materials, 29 (2017) 1601694.

69. R.-B. Wei, Z.-L. Huang, G.-H. Gu, Z. Wang, L. Zeng, Y. Chen, Z.-Q. Liu, Dual-cocatalysts decorated rimous CdS spheres advancing highly-efficient visible-light photocatalytic hydrogen production, Applied Catalysis B: Environmental, 231 (2018) 101-107.
70. L. Andronic, A. Enesca, C. Vladuta, A. Duta, Photocatalytic activity of cadmium doped TiO2 films for photocatalytic degradation of dyes, Chemical Engineering Journal, 152 (2009) 64-71.

Figures

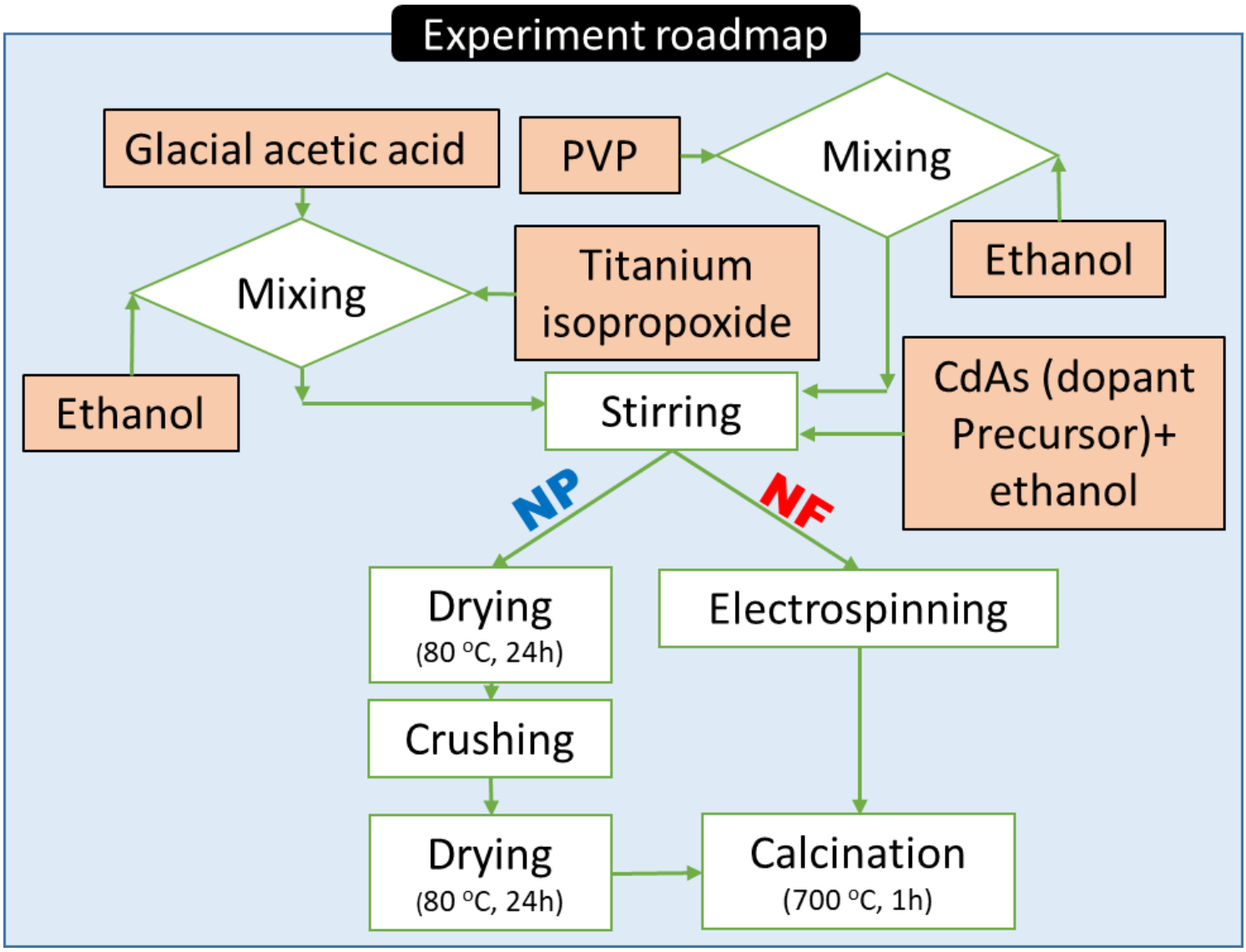

Figure 1

Experimental procedure for Cd-doped TiO_2 nanofibers and nanoparticles preparation.

Figure 2

SEM images for (A) Pristine and (B) 0.5 wt% Cd-doped TiO_2 nanofibers, (C) magnification of 0.5 wt% Cd-doped TiO_2 nanofiber indicating the corrugated/speckled surface of the nanofiber, (D) TEM image of Cd-doped TiO_2 nanofiber indicating the attach of $CdTiO_3$ over the surface of TiO_2 nanofiber

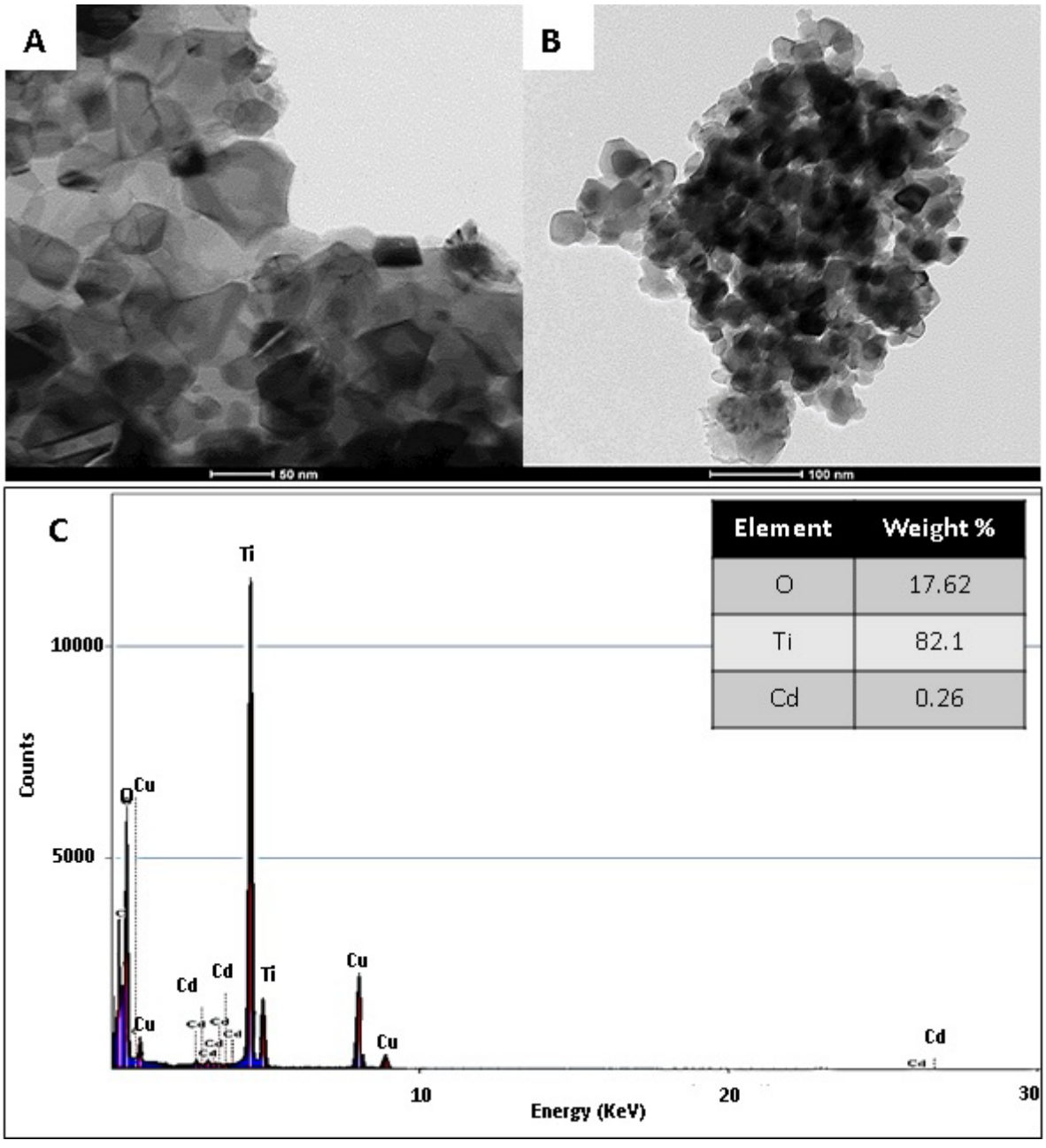

Figure 3

TEM images of (A) TiO_2 nanoparticles, (B) CdO-doped TiO_2 nanoparticles, and (C) The EDX image of CdO doped TiO_2 nanoparticle obtained after atmospheric calcination at 700°C.

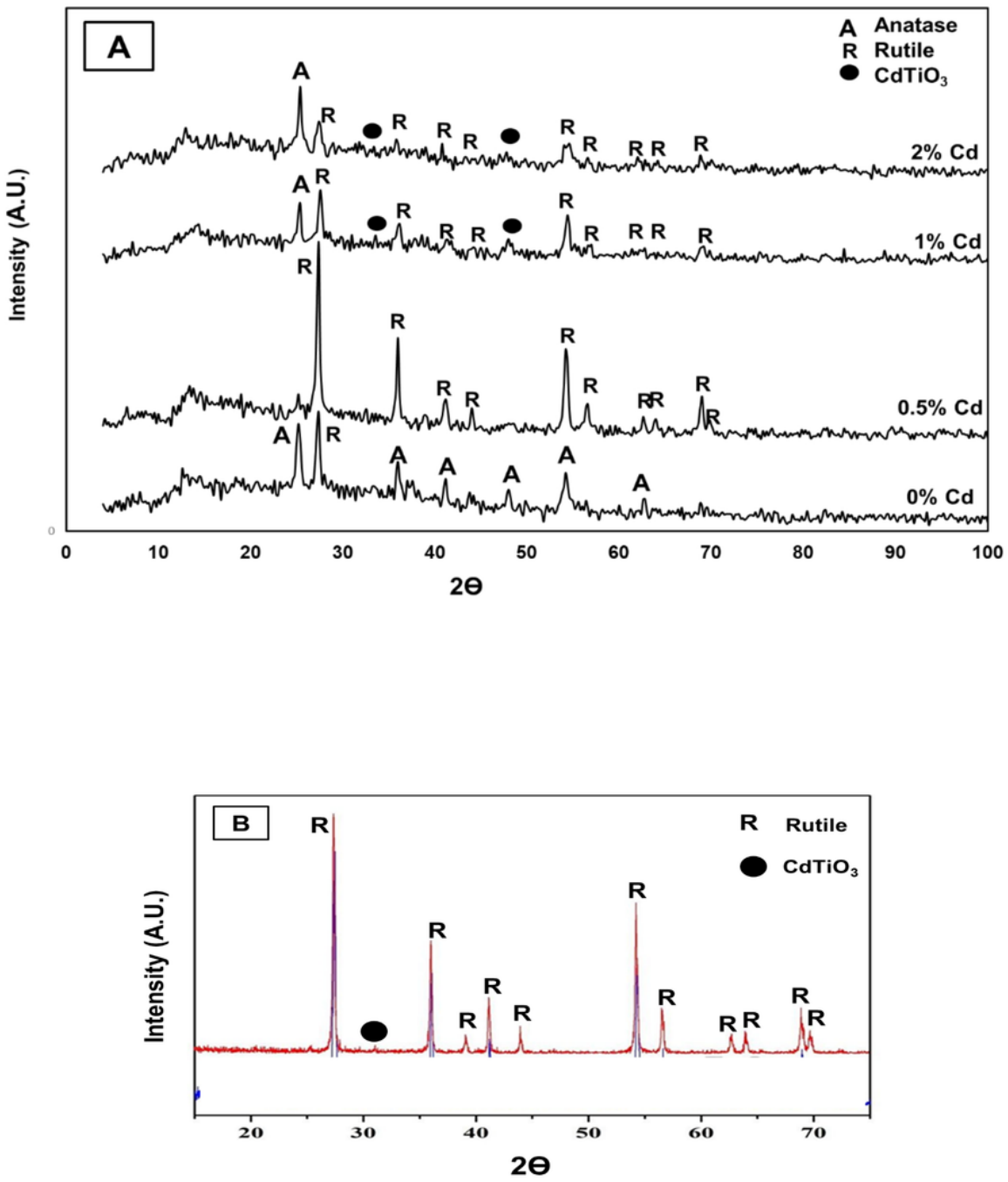

Figure 4

The XRD patterns for (A) pristine and Cd-doped TiO_2 nanofibers and (B) Cd-doped TiO_2 nanoparticles.

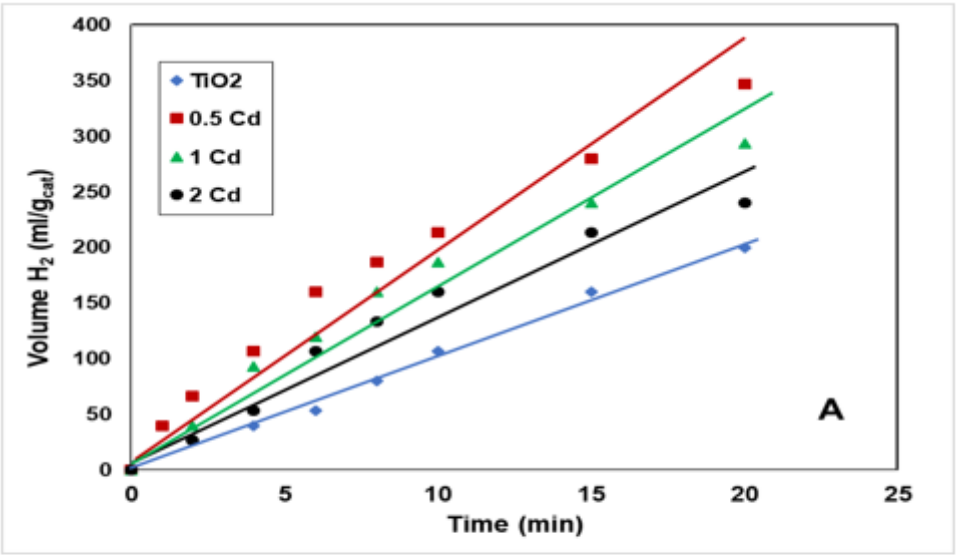

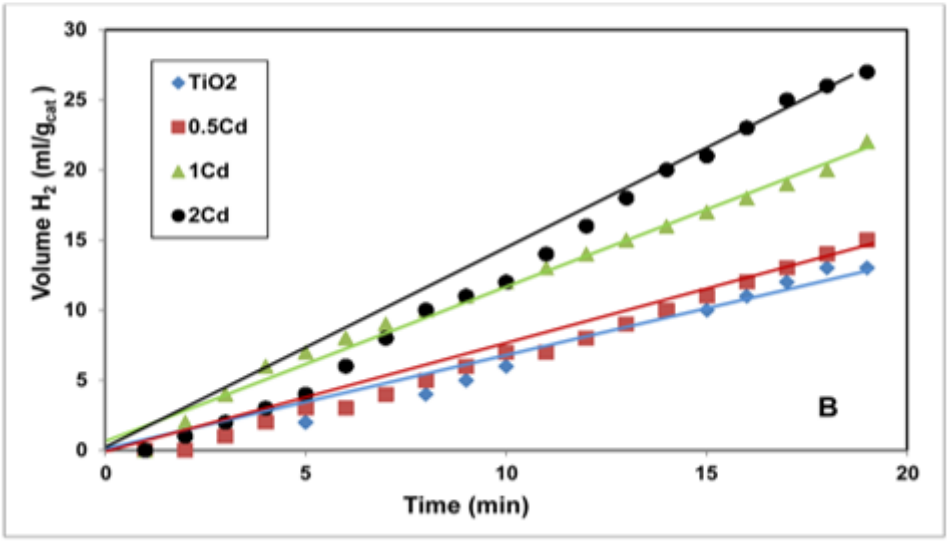

Figure 5

Effect of Cd content on H_2 evolution rate in case of utilizing Cd-doped nanofibers, (A) and nanoparticles, (B) as photocatalyst.

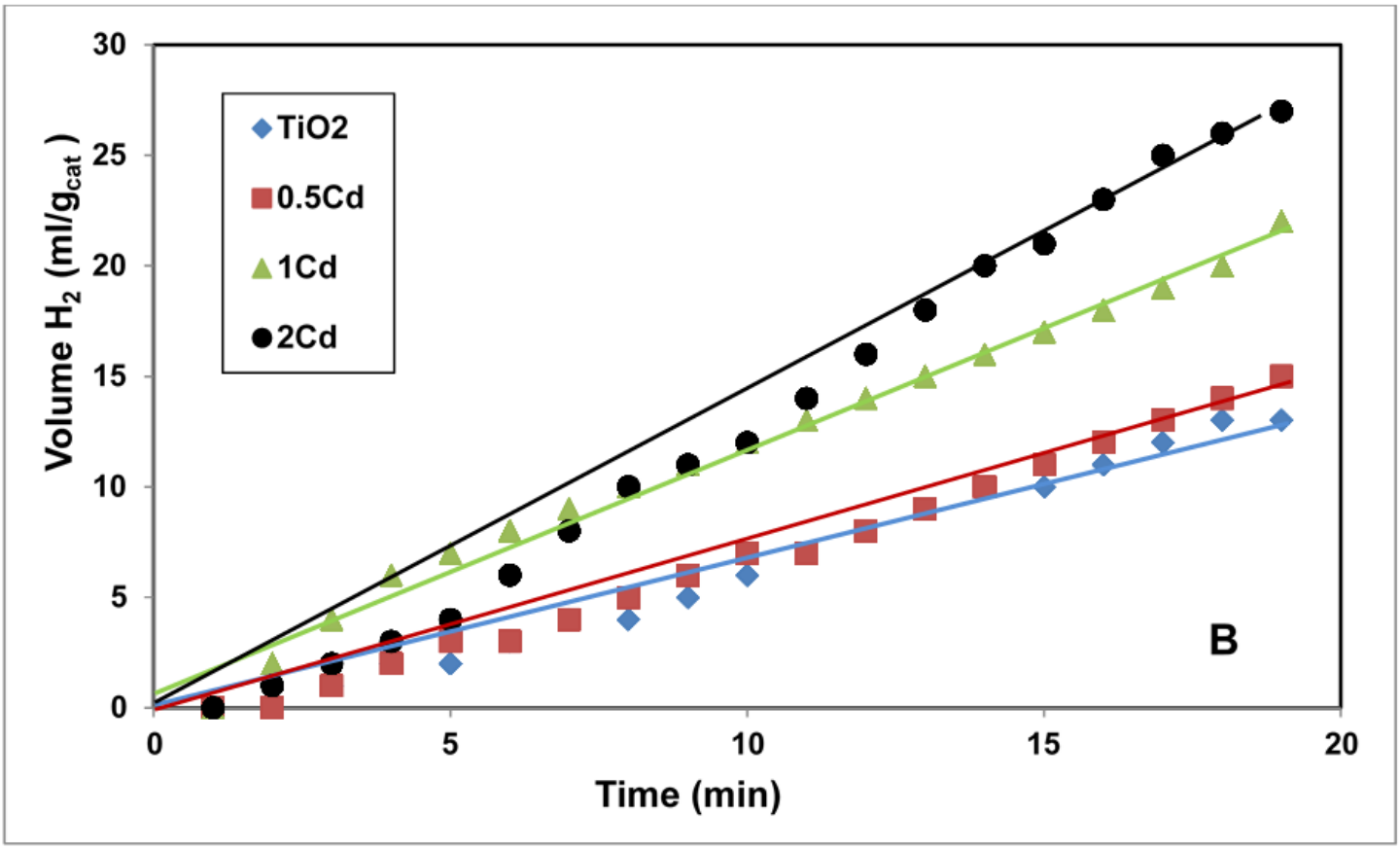

Figure 6

Effect of temperature on Hydrogen Production from water (100 ml) using (0.05 gm) of 0.5 wt % Cd nanofiber.

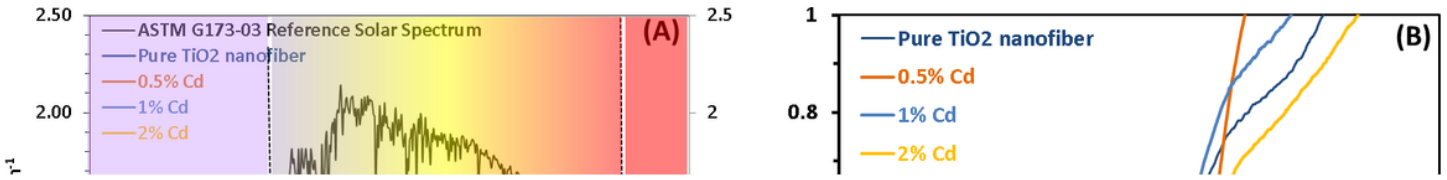

Figure 7

(A) Photon absorption at UV-visible range for the prepared Cd-doped TiO_2 nanofibers compared with pure TiO_2 nanofibers and ASTM G173-03 reference solar spectrum, (B) plot of $(\alpha E_{Photon})^2$ versus E_{Photon} for Cd-doped TiO_2 nanofibers compared with pure TiO_2 nanofiber, the intercepts of the dot lines with the x-axis represent the bandgap energies.

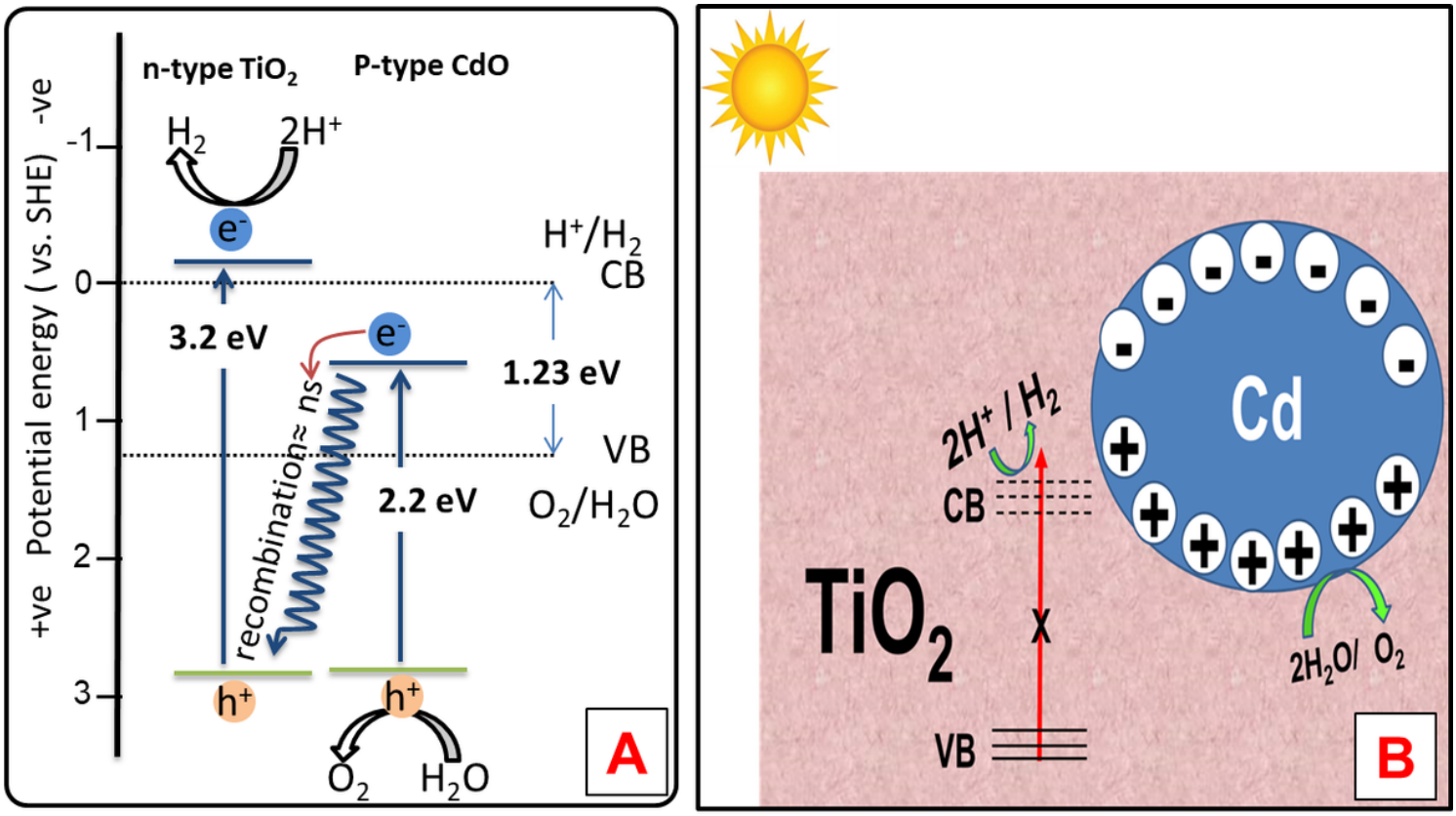

Figure 8

The proposed mechanism for electron transfer and H_2 evolution on Cd-TiO_2 nanofibers(a) Z-scheme mechanism with double charge transfer mechanism and (B) schematic mechanism of water splitting using Cd-doped TiO_2 nanofibers